ADVANCED OPTICAL MATERIALS
www.advopticalmat.de

Intrinsic Chirality and Multispectral Spin-Selective Transmission in Folded Eta-Shaped Metamaterials

Shengyan Yang, Zhe Liu, Haifang Yang, Aizi Jin, Shuang Zhang, Junjie Li,* and Changzhi Gu**

Manipulating light polarization is of fundamental importance in the modern photonic applications such as spectroscopy, laser science, optical communication, quantum information processing, chemical and biological sensing. Polarization control of light is typically achieved by natural chiral or birefringent materials with macroscopic volume due to the weak light–matter interaction. Here, a folded eta-shaped metamaterial that is capable of generating gigantic optical chirality and spectrally breaking the spin degeneracy of optical transmission at multiband is experimentally demonstrated. The intrinsic chiral configuration is achieved by folding the eta-shaped metasurface along the vertical direction to break the mirror symmetries. A remarkable circular dichroism approaching unity is experimentally achieved, with the maximum transmittance exceeding 93%. This is the record high value demonstrated to date for single-layer metasurfaces without diffraction in infrared region. The folded metamaterial provides a straightforward strategy for achieving intrinsic 3D chirality and has great potential for applications in photon-spin selective devices and chiral biomolecule identification.

Chirality, referring to geometrical morphology that cannot superimpose with its mirror image by translational or rotational transformation,[1,2] is ubiquitous in nature and has become an increasingly significant research field since it has important applications in optics, biology, chemistry, pharmaceuticals, and life sciences.[3,4] In the realm of optics, chiral media exhibit distinct optical responses when excited by light with different spin states, and give rise to significant chiral optical effects:[2] circular dichroism (CD) and optical activity (OA). CD refers to the distinct transmissions for left circularly polarized (LCP) and right circularly polarized (RCP) light because of the different absorption and reflectance between RCP and LCP waves, while OA denotes the ability of a chiral medium to rotate the polarization state of linearly polarized light due to the different refraction indices for the LCP and RCP light. Naturally existing chiral materials have been widely used to control the spin states of light in modern polarization systems. However, most media such as sugars, quartz, and amino acids, usually possess a rather weak optical chirality,[2,3] and thus require very long propagation distance to obtain sufficient chiral effect. This severely hinders the miniaturization of optical devices such as lens, beam former, polarizer, waveguide, photonic router, and their applications in nanophotonic and optoelectronic systems.

Compared with the weak chirality of the natural occurring media, elaborately tailored artificial chiral metamaterials consisting of subwavelength constituent elements offer an effective avenue for achieving engineered chirality.[3,4] Chiral metamaterials exhibit orders of magnitude larger chiral optical effects than that of their naturally occurring counterparts, which makes chiral metamaterials highly promising candidates for various applications, including biodetection and chemical analysis,[5,6] chiral light detector,[7] broadband circular polarizer,[8–12] chiral optical imaging,[13,14] nonlinear optics,[15–17] polarization-encrypted data storage,[18] and even negative refractive index materials.[19–21] In the past decades, there have been some significant progresses on manipulating the polarization state of light by 2D and 3D metamaterials.[8–12,22–25] Among the large family of chiral structures, artificial 3D chiral structures have played important roles in spin optics and polarization modulation due to their strong polarization-selective responses.

Dr. S. Yang, Dr. Z. Liu, Prof. H. Yang, A. Jin, Prof. J. Li, Prof. C. Gu
Beijing National Laboratory for Condensed Matter Physics
Institute of Physics
Chinese Academy of Sciences
Beijing 100190, China
E-mail: jjli@iphy.ac.cn; czgu@iphy.ac.cn

Dr. S. Yang, Prof. J. Li, Prof. C. Gu
School of Physical Sciences
CAS Key Laboratory of Vacuum Physics
University of Chinese Academy of Sciences
Beijing 100049, China

Dr. S. Yang
China Electronics Standardization Institute
Beijing 100007, China

Dr. Z. Liu
Niels Bohr Institute
University of Copenhagen
Blegdamsvej 17, DK-2100 Copenhagen, Denmark

Prof. S. Zhang
School of Physics and Astronomy
University of Birmingham
Birmingham B15 2TT, UK
E-mail: s.zhang@bham.ac.uk

The ORCID identification number(s) for the author(s) of this article can be found under https://doi.org/10.1002/adom.201901448.

DOI: 10.1002/adom.201901448

Although complex 3D chiral metamaterials usually possess strong optical chirality, their fabrication is highly challenging and often incompatible with conventional fabrication techniques. Over the past few years, considerable efforts have been devoted to the design and fabrication of 3D chiral metamaterials. For instance, broadband chirality based on 3D gold-helix photonic metamaterials have been demonstrated in the infrared region by using femtosecond direct laser writing technique.[8,9] The minimum realizable features or spatial resolution of this fabrication method are generally in sub-micrometer scale due to the diffraction limit, and thus this method cannot be used to fabricate nanostructures operating in the near-infrared and visible regime. Subsequently, the gold-helix metamaterials have been scaled down to nanoscale by using the focused ion beam– or electron beam–induced deposition method,[10,11] but the material deposition rates are very low, which constrains large-area manufactures. Multilayer metasurfaces were proposed and fabricated by stacking lithography to obtain strong chirality at terahertz and optical frequencies.[12,20] Nevertheless, the stacking lithography requires high-precision alignment and planarization techniques, which leads to very complicated fabrication process. Some other fabrication methods such as on-edge lithography, glancing-angle deposition, and tilted-angle milling technique, have also been employed to fabricate 3D chiral structures.[26–30] However, most of the reported chiral metamaterials are restricted to complex multilayer or sophisticated 3D configurations, which suffer significantly from fabrication challenges, insufficient circular dichroism, low transmittance, or lack of controllability and reproducibility. Recently, the concept of origami or kirigami provides alternative approach to construct 3D structures. Mechanically tunable chirality switching has been implemented by origami metamaterials at microwave regime.[31] Spin-selective transmission has been demonstrated by chiral folded antisymmetric split-ring resonators (SRRs) at infrared region.[32] Nevertheless, achieving intrinsic chirality with multispectral spin selective transmission characteristic in a ultrathin metamaterial is highly desired for multiplexed applications, which still remains a challenging.

In this communication, we experimentally demonstrate a folded eta-shaped metamaterial that possesses gigantic intrinsic 3D chirality and simultaneously supports opposite spin-selective transmission bands in the infrared region. The strong intrinsic optical chirality of the folded metamaterial is introduced by folding the constituent planar metasurface into 3D configurations that break all the mirror symmetries. The folded metamaterial exhibits a sharp contrast in transmission between the opposite spin states of light, with a giant circular dichroism close to unity (0.8) and a maximum transmission >93% of the chosen circularly polarized light. Moreover, numerical and experimental results show that the intrinsic chirality of the folded metamaterials can be effectively modulated via controlling the length of the nanostrip. This ultrathin folded metamaterial may hold potential for various applications such as spin detection, spin-selective optical wavelength multiplexing, ultrathin circular-polarization spectral filters, as well as ultrasensitive sensors for identification of the chirality and structures of biomolecules.

A schematic illustration of the folded eta-shaped metamaterial under investigation is shown in **Figure 1**a. The original eta-shaped metasurface consists of an array of SRRs with asymmetric arms on top of a low-stress, optical transparent, and mechanical stable suspended SiN_x film (Figure S1a, Supporting Information), as illustrated in Figure 1b. The eta-shaped metasurface is fabricated by electron beam lithography followed by a metal deposition procedure (Figure S1b, Supporting Information), with a scanning electron microscope (SEM) image displayed in **Figure 2**a. The original metasurface possesses negligible intrinsic chirality due to the slight symmetry breaking from the SiN_x membrane. It cannot differentiate between the two distinct spin states of light, and therefore the transmission spectra are expected to be identical for LCP and RCP incident light. In order to obtain strong inherent chirality and thus spectrally break the spin degeneracy, we transform each in-plane eta-shaped metasurface into 3D configuration by using focused ion beam–induced deformation techniques.[33–35] The resulting elementary building block of the folded metamaterial is composed of conductively connected vertical SRR and in-plane nanostrip, which has strongly broken mirror symmetry in all directions, as shown in Figure 1c. Figures 1d and 2b show SEM images of the folded eta-shaped metamaterials that are periodically arranged in an array, which manifest the excellent structural quality and uniformity of the fabricated samples. The circular polarization transmittance spectra of the eta-shaped metasurface and folded metamaterial are characterized by Fourier transform infrared (FTIR) spectroscopy (Experimental Section). Full-wave numerical simulation has been performed to investigate the performance of the folded metamaterial.

Figure 2c,d shows the experimentally measured intensity transmission spectra for the RCP and LCP light through the unfolded and folded eta-shaped metamaterial, respectively. For comparison, the simulated intensity transmission spectra are plotted as shown in Figure 2e,f, respectively. The experimental results reveal excellent agreement with rigorous numerical simulations and reproduce all the spectral features. The slight discrepancies in resonant frequencies and shallower depth of the resonances are possibly attributed to the fabrication tolerances. As shown in Figure 2c, two pronounced plasmonic resonances are clearly observed for both LCP and RCP incidence light at 44 and 72 THz, respectively, which is associated with the excitation of the fundamental modes in the eta-shaped metasurface.[36,37] The unfolded metasurface provides the expected nearly identical transmission of LCP and RCP light, which implies that there is no intrinsic chirality in the eta-shaped metasurface. By contrast, when the metasurface is converted to folded configuration, the mirror symmetry of the structure is broken and therefore the chiral optical responses emerge, which provides transmittance of one spin state of incident light while blocking the opposite one. Figure 2d,f shows the transmission spectra of the folded metamaterial for two distinct circular incident waves, respectively, where significant differences are observed in the transmission spectra between LCP and RCP illuminations. It is observed that transmission of LCP incident light is markedly reduced at the lower resonance frequency by the folded metamaterial while almost leaves RCP light transmitted. The measured transmission intensity of the LCP light is highly suppressed with the transmission coefficient of only 0.29 at the resonance frequency of 44.4 THz, while the transmission intensity for RCP light achieves as high as 0.93 at

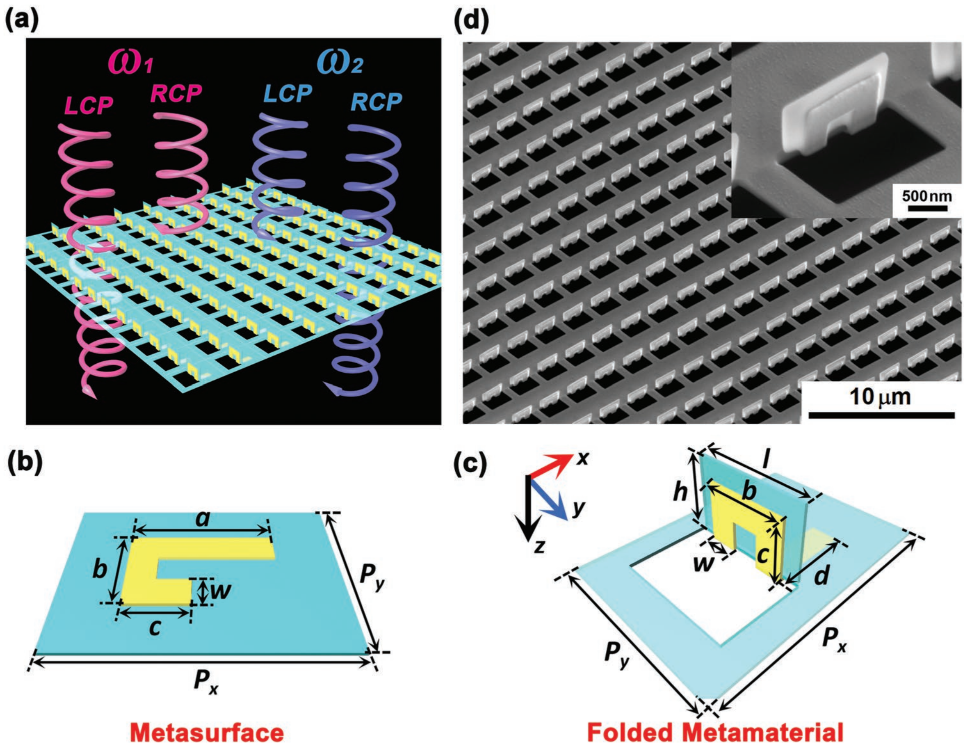

Figure 1. Illustration of the proposed folded eta-shaped metamaterials. a) Schematic diagram illustrates the composite of the folded metamaterial and the illumination configuration. ω_1 and ω_2 represent different operating frequencies, respectively. The functionality of the proposed folded eta-shaped metamaterial is to transmit the designated circularly polarized wave while block the other spin state at multiband. b) Eta-shaped metasurface fabricated on front side of SiN_x film by a facile one-step electron beam lithography and followed by metal deposition processes. c) A perspective schematic representation of a unit cell of metamaterial. The constituent split-ring resonators of the metasurfaces were continuously transformed into 3D folded configurations by focused ion beam–induced deformation techniques. d) Scanning electron microscope image of the fabricated folded metamaterials. Inset: zoomed scanning electron microscopy image showing the well-defined structures, and the scale bar is 500 nm. All the geometric dimensions are: $P_x = 3.2$ µm, $P_y = 2.5$ µm, $a = 1.95$ µm, $b = 1.2$ µm, $c = 850$ nm, $w = 400$ nm, $l = 1.7$ µm, $h = 1.1$ µm, $d = 1.1$ µm. The thickness of gold metasurface is 50 nm.

the resonance (see Figure 2d,f). Interestingly, the situation is reversed at the higher frequency resonance, in which the resonant mode of folded metamaterial reverses its handedness. The transmission spectrum of the folded metamaterial exhibits a strong resonance feature with a transmission minimum of 0.14 at 72.8 THz for RCP illumination, while it leaves a featureless transmission spectrum and maintains high-efficiency transmission of the LCP incident light up to 0.94. The huge discrepancy between the orthogonal circular polarization of transmitted light manifests intrinsic chiral effects in folded metamaterial. At the off-resonant frequencies, the folded metamaterial transmits both LCP and RCP light with equal efficiency. The chirality of the folded metamaterials can be quantitatively characterized by retrieving the CD spectra ($CD = |T_{LCP}| - |T_{RCP}|$, where T_{LCP} and T_{RCP} are the transmission intensity of the LCP and RCP incident light, respectively). The experimental CD spectra of the unfolded metasurface and folded metamaterial from the measured data are plotted in Figure 2g,h, respectively. The simulated CD spectra are also provided in Figure S4 (Supporting Information). The experimental CD for the unfolded metasurface is nearly constant zero over a broad spectrum range, which further confirms that there is no chirality for the planar metasurface. Meanwhile, two reversed resonances appear in the CD spectra of the folded metamaterial, which clearly manifests that the folded metamaterial exhibits the distinct chirality characteristics at multiband. It is shown that the CD magnitude of folded metamaterial becomes minimum and reaches down to −0.64 at the first chiral response, while a much larger CD as high as 0.8 at 72.8 THz is experimentally achieved for the second chiral response, which is unprecedentedly high for a single layer metasurface without diffraction.[12,25–32,38–41] This indicates that the folded metamaterial significantly breaks the spin degeneracy of incident light and achieves high-efficient spin-selective transmission. The folded metamaterial with subwavelength chiral features not only overcomes the limitations of bulk optics and provides opposite chiral spectra discrimination, but also shows the ability of manipulating the spin states of light without the requirement of additional optical components. It is noteworthy that there exists circular polarization conversion between LCP and RCP light due to lack of higher-order (C3 or C4) symmetry, and the conversion effect is considered in the total transmission intensity (see Figure S6 in the Supporting Information).

It is important to note here that the substrate membrane not only influences the dielectric environment of the folded eta-shaped metamaterial and thus produces frequency shift of the chiral resonances, but also affects the impedance matching condition between structure and free space and therefore

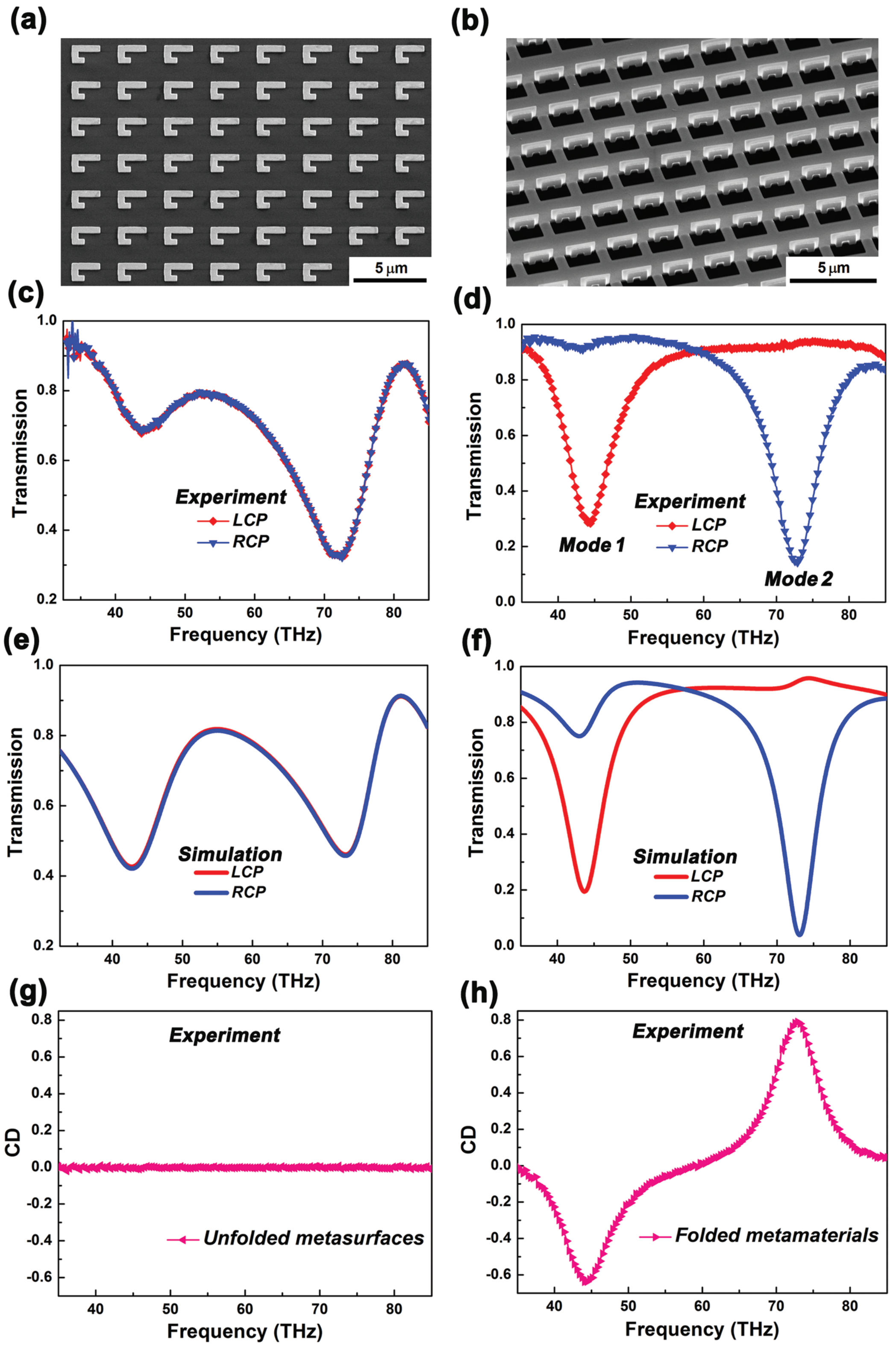

Figure 2. Experimental demonstration of the intrinsic 3D chirality in the folded eta-shaped metamaterials. a) SEM images of unfolded eta-shaped metasurfaces on SiN_x film in top view. b) SEM images of folded eta-shaped metamaterials in 52° oblique view. Experimentally measured transmission spectra of the corresponding c) planar metasurface and d) folded eta-shaped metamaterial for LCP and RCP incident light. Simulated transmission spectra of the corresponding e) planar metasurface and f) folded eta-shaped metamaterial for LCP and RCP incident light. Blue lines and triangles represent RCP transmission, while red lines and diamonds represent LCP transmission, respectively. The retrieved CD spectra of the g) unfolded metasurface and h) folded metamaterial obtained from (c) and (d) are shown in the bottom panels.

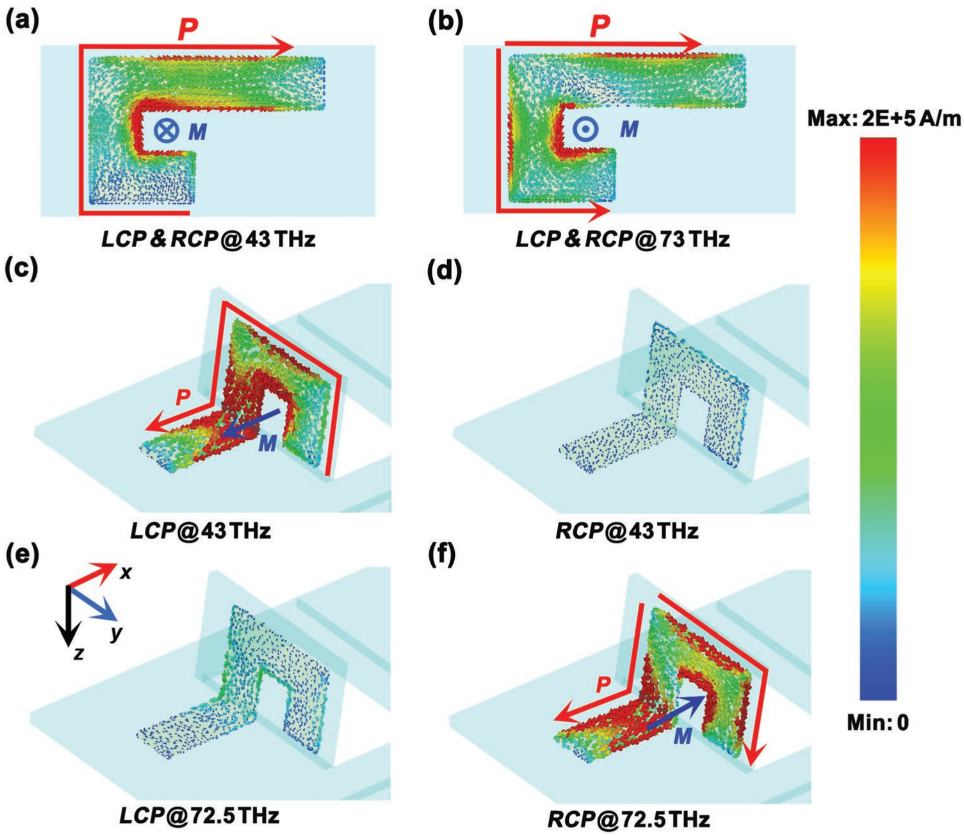

Figure 3. Surface current distributions and dipolar responses of unfolded metasurface and folded metamaterial at chiral resonances. The surface current distributions for the a) lower-frequency and b) higher-frequency resonances in the eta-shaped metasurface under LCP and RCP incidences. The surface current distributions for the c,d) lower-frequency and e,f) higher-frequency chiral resonances in the folded eta-shaped metamaterial under (c, e) LCP and (d, f) RCP incidences. Due to geometrical constraints, the net electric and magnetic moments are always orthogonal for the unfolded metasurface. The induced net electric and magnetic dipoles are parallel and antiparallel for the lower-frequency and higher-frequency chiral responses, respectively. The relative orientations of the generated electric (***P***, red arrow) and magnetic (***M***, blue arrow) dipole moments under illumination are overlaid onto the structures, which are drawn as simple vector arrows for ease of illustration.

influences chiral performance (see Figure S7 in the Supporting Information). Furthermore, it is noticeable that control over the handedness of the folded metamaterial can be readily achieved by changing the connection between the nanostrip and SRR, and consequently the chiral structure is converted to its enantiomer (see Figure S3 in the Supporting Information).

To further reveal the underlying physical mechanism of intrinsic chirality in the folded metamaterials, the surface current distributions at resonant frequencies are plotted and compared under different circular polarization incidences, as shown in **Figure 3**. According to the Rosenfeld criterion,[42,43] optical chirality in intrinsic chiral media is generally a result of the cross-coupling effect between electric and magnetic fields, which can be written as $\sum \vec{P} \cdot \vec{M} \neq 0$, where $\vec{P}$ and $\vec{M}$ denote the electric and magnetic dipoles, respectively. The microscopic origin of the chiral optical response in our folded metamaterials can be interpreted by the cross-coupling of the electric and magnetic fields provided by the electric and magnetic dipoles induced in the in-plane nanostrip and out-of-plane SRR, respectively.

In the case of unfolded metasurface, the metasurface strongly couples with both LCP and RCP incident light, and its transmission property is featured by double broadband resonances (see Figure 2c,e). For the lower frequency resonance occurring at around 43 THz, circular electric current distribution is excited in the eta-shaped metasurface leading to out-of-plane magnetic and in-plane electric dipole excitation, as illustrated in Figure 3a, which corresponds to the lowest even eigenmode of the structure.[36] However, for the higher frequency resonance occurring at around 73 THz, the surface currents are split into two oscillation modes and characterized by the presence of a node in the entire structure, as shown in Figure 3b. A circular current loop and a linear current oscillation are still formed, while the orientation of the magnetic dipole is opposite to that of the lower frequency resonance. Due to the planar configuration, the resultant effective electric and magnetic dipoles are always orthogonal to each other, and therefore no chiral optical response occurs for the unfolded structure.

In the folded metamaterial, the deformation of the metasurface leads to realignment of the magnetic and electric dipoles that could be parallel or antiparallel to each other, which leads to the generation of distinct coupling behavior between the induced magnetic and electric responses, and consequently different chiral optical behaviors. For the first chiral response (Mode 1), the folded metamaterial strongly couples to LCP incident light, resulting in oscillating currents on the in-plane nanostrip that can be regarded as an electric dipole. Meanwhile, the oscillation of circular current loop generated on the vertical SRR that gives rise to a magnetic dipole in the same direction as the electric dipole, as illustrated in Figure 3c. In this case, there exists a strong in-phase magnetoelectric coupling between the electric field and magnetic field propagating through the folded metamaterial and consequently leads to a strong chiral optical effect. However, in the case of RCP illumination, the induced currents from the magnetic dipole and the electric dipole interfere destructively, and as such the folded metamaterial has a weak interaction with the incident RCP light, as shown in Figure 3d. This results in the breaking of degeneracy between the two spin states, i.e., the absorption is increased for one spin state and reduced for the other. In the case of the second chiral resonance (Mode 2), the surface current distributions plotted in Figure 3f reveals that major part of the electromagnetic energy are confined into the folded structures and strong resonance are stimulated by external RCP light. The effective electric and magnetic dipoles induced by the incident RCP light are antiparallel with each other (oscillating (π) out of phase), and this fact contributes to the reversed chiral response compared to that of the lower frequency resonance (Mode 1). The subtle surface current distributions plotted in Figure 3e reveals that the interaction between the folded metamaterial and external LCP light is very weak, which implies that LCP light could transmit through the folded metamaterial with weak attenuation. As a result, the distinct coupling mechanisms between the electric and magnetic dipoles generated by the nanostrip and folded SRR yield completely reversed chiral optical responses of the folded metamaterial at different frequencies.

It is noticed that the intrinsic chirality of the folded eta-shaped metamaterial is primarily determined by the configuration of the unit cell, and periodic arrangement of building elements result in dramatic enhancement of the chiral optical responses due to the collective excitation of the unit cells (see Figure S5 in the Supporting Information). Moreover, the spatial electric field distribution around the folded structures for both LCP and RCP incidences are provided and analyzed in Figure S8 (Supporting Information), which further confirm the origin of the chirality of the folded structures and consistent with the current distribution analysis.

Achieving a simple strategy for the continuous engineering of chiral optical responses plays an irreplaceable role in practical applications involving spin optics and sensing. Since the distinct chiral responses are introduced by the coupling between the in-plane nanostrip and out-of-plane SRR, the evolution of the CD spectra of the folded metamaterial with the length of the in-plane nanostrip (d) is further investigated. In order to see how spectra and mode energies change as a function of d, **Figure 4**a,b shows the evolution of calculated CD spectra of the folded eta-shaped metamaterials as a sweep of the nanostrip length from 0.4 to 1.6 μm. The experimentally measured CD

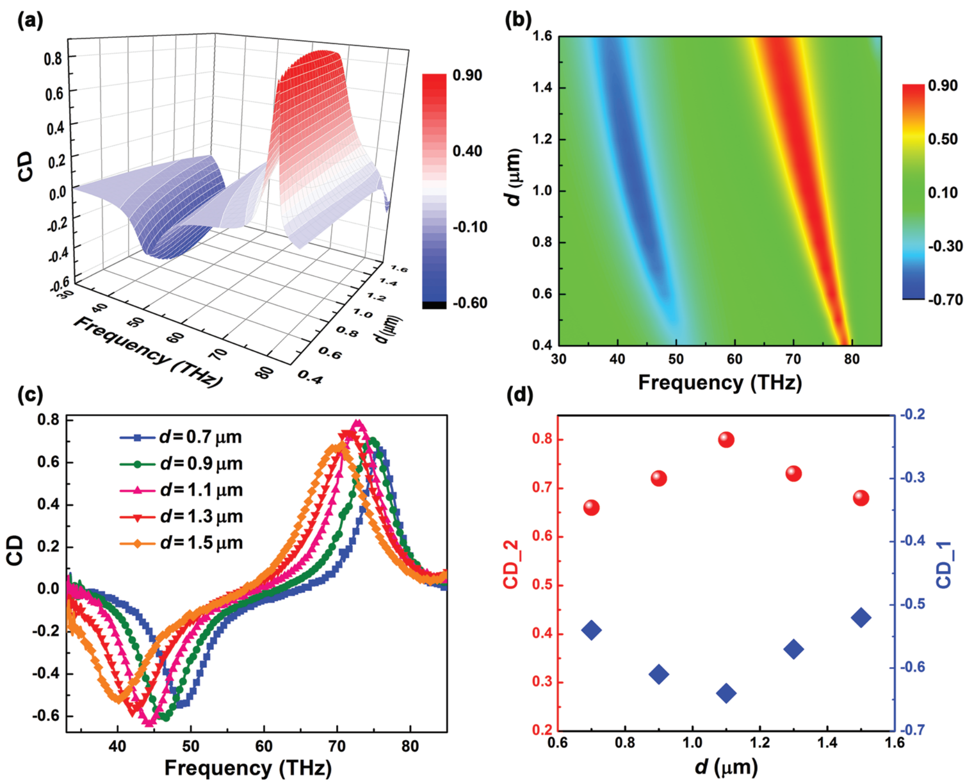

Figure 4. Circular dichroism of the folded eta-shaped metamaterials with different length of the nanostrip. a,b) Simulated CD spectra of the folded eta-shaped metamaterial as a function of the nanostrip d. The red and blue regions represent the frequency range where the chirality is reversed. c) Measured CD spectra of the folded eta-shaped metamaterials with different nanostrip lengths of d. d) CD values of the folded eta-shaped metamaterials at the resonance frequency for different lengths of d. The blue square dots denote the CD value of the first chiral response and the red circular dots represent the CD value of the second chiral response, respectively. The numerical results show good agreement with the experimental observations.

curves for different nanostrip lengths of the folded metamaterial are plotted in Figure 4c. The corresponding experimentally measured CD values at the chiral resonance versus the length of the nanostrip are depicted in Figure 4d. The simulation results are in good agreement with the experimental observations that reproduces the modulation trend of CD data. Evidently, both the reversed chiral resonances simultaneously occur in the spectra and reveal an explicit modulations trend with varied geometrical parameter (*d*), as shown in Figure 4a–c. The resonant frequencies gradually redshift as the increase of the in-plane nanostrip length, indicating that the operating frequencies of the folded metamaterial can be effectively tuned by adjusting the nanostrip length. The CD value for the first chiral response remains negative as the length of the antenna varied, while it keeps positive for the second chiral response. The magnitude of the CD peak for the two distinct chiral responses gradually increases when tailoring the length of the nanostrip from 0.4 to 1.1 µm, which indicates that the chiral optical responses are significantly enhanced as the nanostrip lengths increase and reach their maximum at $d \approx 1.1$ µm. Further increasing the length of the nanostrip beyond a critical value leads to a slightly weakened CD value. Therefore, it is clear that the chirality of the designed folded metamaterial can be modulated continuously by changing the length of the nanostrip across a broad waveband. Controlling the electric and magnetic couplings by tuning the length of the nanostrip provides a powerful method to manipulate the chiral properties of folded metamaterials. It is worth mentioning that the chiral responses can also be controlled by the geometry of the out-of-plane SRR, which has an equivalently effect on tailoring the magnetic dipole moment. The folded metamaterials exhibit excellent tunability of chiral properties by tailoring the geometrical parameters, which means that it enables the precise control of the chiral responses and therefore provides a new strategy for engineered multiple chiral responses as needed.

Here, we accomplish intrinsic chiral effects analogous to nature occurring chiral media with deeply subwavelength thickness, high modulation flexibility, and excellent performance. The folded metamaterial switches its functionality between transparent and opaque states for circular polarized light at different frequencies. Hence, the folded metamaterials can act as dual-band bifunctional circular polarizers that filter different spin states at two resonances. Moreover, the operating principles and fabrication techniques of folded metamaterials may be readily scaled down to visible region by reducing the unit-cell size (or choosing low refractive-index membrane) or extended to longer wavelengths for a variety of significant applications in the far-infrared and terahertz spectral range, for which advanced optical elements for circular polarization control (e.g., quarter wave plates or circular polarizers) are urgently needed. In addition, the use of multiple inclusions within each unit cell may be explored to further increase the operational bands. Furthermore, the folded metamaterials can be further embedded in optically or thermally sensitive materials, allowing the active modulation of chiral optical responses, or photoluminescent media, resulting in chirality selective enhancement of photon emission.

In summary, a novel folding eta-shaped metamaterial is proposed and fabricated to achieve remarkable intrinsic 3D chirality and simultaneously support spin-selective-transmission frequency multiplexing for the infrared spectra. Most remarkably, the experimentally achieved maximum circular dichroism is approximate unity (0.8), with >93% of the selected circularly polarized light being transmitted. The intrinsic chirality is realized by breaking all the mirror symmetries via transforming the metasurface into 3D configuration. The excitation of both normal and tangential currents in the structure leads to distinct magnetic dipole parallel or antiparallel to the in-plane electric dipole, resulting in distinct chiral resonances. Moreover, the chiral responses in the folded metamaterial can be effectively controlled by simply adjusting the length of the in-plane nanostrip. The folded metamaterial provides a robust and unique method for engineered 3D intrinsic chirality and offers intriguing possibilities for applications in compact multiband circular polarizer, polarization transformer, spin recognition, chiral imaging, and optical information processing.

Experimental Section

Nanofabrication: Polymethyl methacrylate resist was first spin-coated on the front side of the 100 nm thick low-stress suspended SiN_x window, and baked at 180 °C for 1 min, after which the front side of the SiN_x window was directly patterned with eta-shaped structures by electron beam lithography. Subsequently, a 50 nm thick gold film was deposited onto the front resist layer using electron beam evaporation method and then followed by an acetone lift-off procedure to obtain gold patterns (Figures 1b and 2a). After that, 50 nm aluminum film was deposited onto the back side of the SiN_x window by electron beam evaporation. Then, focused ion beam system (Helios 600i, FEI) was sequentially utilized to etch narrow slits on the SiN_x film around the SRR patterns and form SiN_x membrane sheets (see Figure S1c in the Supporting Information). The sample was flipped over (Figures S1d and S2b, Supporting Information) before folding processing in order to prevent the metasurfaces from damaging by the ion beam. Then, focused ion beam stress–induced deformation techniques were utilized to fold the patterns up via continuously scanning the bottom edge of the SiN_x sheets and accomplish the construction of the 3D structures (Figures S1e and S2c, Supporting Information). Finally, the aluminum conductive layer on the back side was removed by wet etching in NaOH solution. The acceleration voltage of focused gallium ions was 30 kV, and the ion beam current was 40 pA. The footprint of the fabricated sample was more than 100×100 µm^2.

Optical Characterization: Both the fabricated unfolded metasurface and folded metamaterials were characterized by a FTIR spectroscopy microscope (Bruker Vertex 80) with a custom ordered Mid-IR achromatic quarter waveplate (B. Halle Nachfl. GmbH) inserted into the beam path between a linear polarizer and the sample. A Globar was used as the mid-infrared light source and a ZnSe polarizer was used to generate the liner polarized light. The transmitted light was collected using a liquid nitrogen cooled mercury cadmium telluride detector. The measurements were carried out at normal incidence with the incident light propagating along the +*z*-direction. All the spectra were measured with a resolution of 4 cm^{-1} and 128 scans. All the transmission spectra were normalized to the transmission spectra of air.

Numerical Simulations: To clarify the mechanism of the intrinsic chiral optical responses observed in the experiments, the unfolded metasurfaces and folded metamaterials were theoretically analyzed based on finite element method. The full wave simulations (transmission spectra and surface current distributions) were conducted, performed by a commercially available software (CST Microwave Studio) using a finite-element frequency-domain solver with unit-cell boundary conditions in the *x*–*y*-plane and Floquet ports in the *z*-direction for terminating the domain. In the simulations, at least 5 mesh steps per wavelength were used to guarantee the accuracy of the calculated results. The dispersion function of gold was described by the Drude model with plasma frequency $\omega_p = 1.37 \times 10^{16}$ s^{-1} and the damping constant $\gamma = 1.2 \times 10^{14}$ s^{-1}.[8,44] The permittivity of the SiN_x was taken as 4.84, and the material loss was ignored in simulations which would not affect the overall results.

Supporting Information

Supporting Information is available from the Wiley Online Library or from the author.

Acknowledgements

S.Y. and Z.L. contributed equally to this work. This work was supported by the National Key Research and Development Program of China under Grant Nos. 2016YFA0200400 and 2016YFA0200800; the National Natural Science Foundation of China under Grant Nos. 91323304, 11674387, 11504414, 11574369, 11574385, 11574368, 11434017, and 61390503; the Strategic Priority Research Program and Key Research Program of Frontier Sciences, CAS, Grant Nos. XDB07020200 and QYZDJ-SSW-SLH042; the European Research Council Consolidator Grant (TOPOLOGICAL).

Conflict of Interest

The authors declare no conflict of interest.

Keywords

folded metamaterials, intrinsic chirality, multispectral spin-selective transmission, subwavelength optics

Received: August 23, 2019
Revised: October 7, 2019
Published online: December 18, 2019

[1] L. Kelvin, *Baltimore Lectures on Molecular Dynamics and the Wave Theory of Light*, Clay and Sons, London **1904**.
[2] L. D. Barron, *Molecular Light Scattering and Optical Activity*, Cambridge University Press, Cambridge **2004**.
[3] V. K. Valev, J. J. Baumberg, C. Sibilia, T. Verbiest, *Adv. Mater.* **2013**, *25*, 2517.
[4] J. T. Collins, C. Kuppe, D. C. Hooper, C. Sibilia, M. Centini, V. K. Valev, *Adv. Opt. Mater.* **2017**, *5*, 1700182.
[5] E. Hendry, T. Carpy, J. Johnston, M. Popland, R. V. Mikhaylovskiy, A. J. Lapthorn, S. M. Kelly, *Nat. Nanotechnol.* **2010**, *5*, 783.
[6] Y. Zhao, A. N. Askarpour, L. Sun, J. Shi, X. Li, A. Alu, *Nat. Commun.* **2017**, *8*, 14180.
[7] W. Li, Z. J. Coppens, L. V. Besteiro, W. Wang, A. O. Govorov, J. Valentine, *Nat. Commun.* **2015**, *6*, 8379.
[8] J. K. Gansel, M. Thiel, M. S. Rill, M. Decker, K. Bade, V. Saile, M. Wegener, *Science* **2009**, *325*, 1513.
[9] J. Kaschke, L. Blume, L. Wu, M. Thiel, K. Bade, Z. Yang, M. Wegener, *Adv. Opt. Mater.* **2015**, *3*, 1411.
[10] M. Esposito, V. Tasco, M. Cuscunà, F. Todisco, A. Benedetti, I. Tarantini, M. De Giorgi, D. Sanvitto, A. Passaseo, *ACS Photonics* **2015**, *2*, 105.
[11] D. Kosters, A. Hoogh, H. Zeijlemaker, H. Acar, N. Rotenberg, L. Kuipers, *ACS Photonics* **2017**, *4*, 1858.
[12] Y. Zhao, M.A. Belkin, A. Alu, *Nat. Commun.* **2012**, *3*, 870.
[13] M. Khorasaninejad, W. T. Chen, A. Y. Zhu, J. Oh, R. C. Devlin, D. Rousso, F. Capasso, *Nano Lett.* **2016**, *16*, 4595.
[14] Y. Chen, J. Gao, X. Yang, *Adv. Opt. Mater.* **2019**, *7*, 1801467.
[15] M. Ren, E. Plum, J. Xu, N. I. Zheludev, *Nat. Commun.* **2012**, *3*, 833.
[16] S. P. Rodrigues, S. Lan, L. Kang, Y. Cui, W. Cai, *Adv. Mater.* **2014**, *26*, 6157.
[17] S. P. Rodrigues, S. Lan, L. Kang, Y. Cui, P. W. Panuski, S. Wang, A. M. Urbas, W. Cai, *Nat. Commun.* **2017**, *8*, 014602.
[18] Y. Chen, X. Yang, J. Gao, *Light: Sci. Appl.* **2019**, *8*, 45.
[19] J. B. Pendry, *Science* **2004**, *306*, 1353.
[20] S. Zhang, Y. S. Park, J. Li, X. Lu, W. Zhang, X. Zhang, *Phys. Rev. Lett.* **2009**, *102*, 023901.
[21] E. Plum, J. Zhou, J. Dong, V. A. Fedotov, T. Koschny, C. M. Soukoulis, N. I. Zheludev, *Phys. Rev. B* **2009**, *79*, 035407.
[22] S. C. Jiang, X. Xiong, Y. S. Hu, Y. H. Hu, G. B. Ma, R. W. Peng, C. Sun, M. Wang, *Phys. Rev. X* **2014**, *4*, 021026.
[23] S. C. Jiang, X. Xiong, P. Sarriugarte, S. W. Jiang, X. B. Yin, Y. Wang, R. W. Peng, D. Wu, R. Hillenbrand, X. Zhang, M. Wang, *Phys. Rev. B* **2013**, *88*, 161104(R).
[24] X. Xiong, Y. S. Hu, S. C. Jiang, Y. H. Hu, R. H. Fan, G. B. Ma, D. J. Shu, R. W. Peng, M. Wang, *Appl. Phys. Lett.* **2014**, *105*, 201105.
[25] B. Tang, Z. Li, E. Palacios, Z. Liu, S. Butun, K. Aydin, *IEEE Photonics Technol. Lett.* **2017**, *29*, 295.
[26] K. Dietrich, D. Lehr, C. Helgert, A. Tünnermann, E. B. Kley, *Adv. Mater.* **2012**, *24*, OP321.
[27] A. G. Mark, J. G. Gibbs, T. C. Lee, P. Fischer, *Nat. Mater.* **2013**, *12*, 802.
[28] Y. Chen, J. Gao, X. Yang, *Nano Lett.* **2018**, *18*, 520.
[29] M. Zhang, V. Pacheco-Peña, Y. Yu, W. Chen, N. J. Greybush, A. Stein, N. Engheta, C. B. Murray, C. R. Kagan, *Nano Lett.* **2018**, *18*, 7389.
[30] Y. He, G. K. Larsen, W. Ingram, Y. Zhao, *Nano Lett.* **2014**, *14*, 1976.
[31] Z. Wang, L. Jing, K. Yao, Y. Yang, B. Zheng, C. M. Soukoulis, H. Chen, Y. Liu, *Adv. Mater.* **2017**, *29*, 1700412.
[32] S. Yang, Z. Liu, S. Hu, A. Z. Jin, H. Yang, S. Zhang, J. Li, C. Gu, *Nano Lett.* **2019**, *19*, 3432.
[33] S. Yang, Z. Liu, L. Jin, W. Li, S. Zhang, J. Li, C. Gu, *ACS Photonics* **2017**, *4*, 2650.
[34] Z. Liu, A. Cui, J. Li, C. Gu, *Adv. Mater.* **2019**, *31*, 1802211.
[35] J. Li, Z. Liu, *Nanophotonics* **2018**, *7*, 1637.
[36] S. Yang, Z. Liu, X. Xia, Y. E, C. Tang, Y. Wang, J. Li, L. Wang, C. Gu, *Phys. Rev. B* **2016**, *93*, 235407.
[37] S. Yang, C. Tang, Z. Liu, B. Wang, C. Wang, J. Li, L. Wang, C. Gu, *Opt. Express* **2017**, *25*, 15938.
[38] B. Frank, X. Yin, M. Schäferling, J. Zhao, S. M. Hein, P. V. Braun, H. Giessen, *ACS Nano* **2013**, *7*, 6321.
[39] Z. Li, M. Gokkavas, E. Ozbay, *Adv. Opt. Mater.* **2013**, *1*, 482.
[40] W. Ye, X. Yuan, C. Guo, J. Zhang, B. Yang, S. Zhang, *Phys. Rev. Appl.* **2017**, *7*, 054003.
[41] J. Hu, X. Zhao, Y. Lin, A. Zhu, X. Zhu, P. Guo, B. Cao, C. Wang, *Sci. Rep.* **2017**, *7*, 41893.
[42] L. Rosenfeld, *Z. Phys.* **1929**, *52*, 161.
[43] M. Schäferling, *Chiral Nanophotonics*, Springer International Publishing, Switzerland **2017**.
[44] M. A. Ordal, L. L. Long, R. J. Bell, S. E. Bell, R. R. Bell, R. W. Alexander, C. A. Ward, *Appl. Opt.* **1983**, *22*, 1099.